**Whole brain network analysis of neural synchrony and information flow during transition from wakefulness to light non-rapid eye movement sleep**

Joline M. Fan[1]*, Kiwamu Kudo[2,3], Parul Verma[2], Kamalini G. Ranasinghe[1], Hirofumi Morise[2,3], Anne M. Findlay[2], Keith Vossel[1,5], Heidi E. Kirsch[1,2], Ashish Raj[2], Andrew D. Krystal[4,†], Srikantan S. Nagarajan[2,†]

[†]These authors contributed equally to this work.

**Author Affiliations**

[1]Department of Neurology, University of California San Francisco, San Francisco CA, USA

[2]Department of Radiology and Biomedical Imaging, University of California San Francisco, San Francisco, USA

[3]Medical Imaging Center, Ricoh Company, Ltd., Kanazawa, Japan

[4]Department of Psychiatry, University of California San Francisco, San Francisco CA, USA

[5]Mary S. Easton Center for Alzheimer's Disease Research, Department of Neurology, David Geffen School of Medicine, University of California Los Angeles, Los Angeles, CA, USA

**Correspondence to:** Joline M. Fan, MD
505 Parnassus Ave, Box 0114
San Francisco, CA 94158
joline.fan@ucsf.edu

**Keywords:** Non-rapid eye movement (NREM), functional connectivity, directional phase transfer entropy, sleep, default mode network

**ABSTRACT**

Sleep is a highly stereotyped phenomenon, requiring robust spatial and temporal coordination of neural activity. How the brain coordinates neural activity with sleep onset can provide insight into the physiological functions subserved by sleep and pathologic phenomena associated with sleep onset. Here, we quantified whole-brain network changes during the transition from wake to non-rapid eye movement (NREM) sleep using magnetoencephalography imaging in healthy subjects. The sleep transition was identified to be encoded in spatially and temporally specific patterns of local and long-range neural synchrony. Patterns of information flow revealed that mesial frontal regions receive hierarchically organized inputs from broad cortical regions upon sleep onset. Finally, biophysical neural mass modeling demonstrated spatially heterogeneous properties of cortical excitation-to-inhibition from wake to NREM. Together, these findings provide evidence for the structured corticocortical modulation in sleep-wake behavior and demonstrate the orchestration of local and long-range, frequency-specific cortical interactions that are fundamental to sleep onset.

## INTRODUCTION

The transition to sleep involves a set of neural processes that reliably promotes a behavioral state-change and sets the stage for essential functions of sleep. Classical lesion and stimulation-based studies have identified sleep-wake transitions as modulated by distributed circuits originating in the brainstem and extending to the hypothalamus, thalamus, and basal forebrain[1,2]. Such bottom-up regulation of sleep and wake has led to a model whereby cortical structures are simultaneously activated by subcortical structures during global state transitions. More recent studies, however, have identified the presence of local cortical dynamics during sleep[3–7] and furthermore suggest that the neocortex may even play a top-down role in sleep-wake regulation[8,9]. To this end, we pose the fundamental question – are there structured corticocortical functional interactions during sleep? If so, this structure may play a critical role in cortically-based physiologic phenomena, such as emotional regulation[10–12], memory consolidation[13–15], and recovery[16], and pathologic phenomena of sleep onset, such as state-dependent epileptic spiking or insomnia.

For many decades, sleep electrophysiology has been characterized by recordings from a limited number of scalp electrodes, as traditionally used in polysomnography. Meanwhile, fMRI/PET[17–19] studies have provided key anatomical insights on whole-brain neural activation patterns of sleep. Such large-scale network analyses primarily using fMRI have revealed widespread increases in corticocortical connectivity and decreases in thalamocortical connectivity during light non-rapid eye movement (NREM)[20–22]; deep NREM has been associated with widespread decreases in functional connectivity (FC) and increased thalamocortical connectivity[20,21]. The diffuse increase in corticocortical FC from wakefulness to light NREM has been hypothesized to lead to reduced information integration, underpinning the loss of consciousness with sleep[23,24]. While fMRI/PET offer

high spatial resolution, these imaging modalities indirectly probe neural activity (e.g., fMRI measures blood flow and PET measures neural metabolic rate) and are limited by low temporal resolution.

Complementing prior fMRI methods, several key MEG/EEG[25–27] studies have elucidated frequency-specific patterns with sleep onset, including the robust increase in low frequency oscillations in midline anterior brain regions, which later propagate posteriorly[26]. The increased corticocortical connectivity with sleep onset has been furthermore observed across multiple frequency bands using band-limited power correlations of MEG/EEG sensor time series[28]. To date, however, MEG/high-density EEG studies have been limited by the lack of a comprehensive assessment of simultaneous local and long-range neuronal synchrony and information flow with transition from wakefulness to sleep. Furthermore, amidst findings of global increases and decreases in FC, salient long-range cortical interactions have not previously been observed, which may reflect prior methodological limitations including: uninterpretable measures of connectivity due to the lack of source reconstruction[28]; temporal blurring due to the lack of simultaneous EEG for sleep-scoring in MEG studies; and correlational connectivity methods that may introduce effects of volume conduction or other sources of spurious connectivity.

In this study, we sought to identify local and long-range cortical structure that underlie global state transitions. We pursued three aims: 1) to determine which cortical areas are preferentially activated by local synchronization during sleep onset using MEG imaging; 2) to determine what cortical regions facilitate long-range synchronization observed upon the transition to sleep; and 3) to infer mechanisms underlying the observed network physiology using biophysical models. We hypothesized that there are frequency-specific, spatial patterns of corticocortical synchronization and information flow upon transition to sleep. Furthermore, in the context of spatially-specific cortical patterns of neural synchronization, we hypothesized that the underlying corticocortical structure represents spatially heterogeneous excitatory-to-inhibitory activity during light NREM. To test these hypotheses, we leveraged the high spatial and temporal sensitivity of MEG imaging to quantify

spatial-temporal patterns of local and long-range neural synchrony across oscillatory frequencies in healthy individuals. We employed simultaneous EEG recordings to enable accurate standardized sleep staging of corresponding MEG data and examined three complementary metrics (i.e. spectral power, functional connectivity, and information flow) using source-reconstructed time courses. Finally, we performed computational modeling of the underlying neurophysiology using a deterministic neural mass model (NMM) to quantify the cortical excitation-to-inhibition balance across sleep-wake states. Our findings reveal the orchestration of large-scale cortical interactions that are intrinsic to sleep onset and homeostasis, which provide additional evidence for the role of corticocortical modulation in sleep.

## MATERIALS AND METHODS

*Study cohort*

MEG and simultaneously obtained scalp EEG data were obtained from a set of 19 healthy elderly individuals (age, mean 63.6 y [SD 11.2]; gender, female 11 of 19 [78.6%]). All participants underwent a complete history and physical examination. Exclusion criteria for this healthy cohort included any neurologic disorders by history or abnormal neurologic findings by exam. In addition, exclusion criteria included use of any chronic or acute neuroactive medications, including neuroleptics, benzodiazepines, SSRI/SNRIs, or sedatives. Inclusion criteria included achieving at least an aggregate of 60 seconds within each sleep-wake state (W, N1 and N2, segmented into 15 second epochs, see below) during the EEG/MEG study. Fourteen participants met inclusion criteria and were included into the study. In all subjects, the use of these data for research was approved by the University of California Institutional Review Board, and all subjects provided written informed consent prior to data collection.

*Data acquisition and preprocessin*g

EEG/MEG data were obtained for a period of 50-70 minutes of resting state, recorded at a sampling rate of 600 Hz. Before the start of the recording, subjects were instructed to close their eyes and attempt to sleep. Subjects did not engage in any tasks during the recording. Raw EEG/MEG traces were chunked into 15 second epochs. Each epoch was visually inspected and rejected if there was presence of movement artifacts. In a subset of subjects with metallic artifacts from non-cranial implants, a digital signal subspace project (DSSP) algorithm was used for denoising[29]. Epochs were scored into the appropriate sleep states based on scalp EEG criteria and using two-person validation according to American Academy of Sleep Medicine (AASM) criteria. The 15 second epochs of MEG data were then concatenated together to achieve at minimum, a 60 second time series representing each behavioral state. A maximum of the first eight artifact-free epochs, e.g. 120 second sensor time, were utilized in this analysis. Prior work demonstrated that 60 seconds of resting wake state is an adequate duration to reliably achieve stationarity for MEG time series[30]. Source reconstruction

was performed using adaptive spatial filtering methods[31] at an individual subject level, yielding voxel level source time series. Source reconstructions were co-registered to MNI template, and regional level time courses were extracted with alignment to the Brainnetome atlas[32], parcellated into 210 cortical regions of interests (ROIs). The data analysis pipeline is illustrated in Fig 1s.

*Data analysis and neural mass model*

Time series data were bandpass filtered into the following frequency bands: delta (1-4 Hz), theta (4-8 Hz), alpha (8-12 Hz), sigma (12-15 Hz), and beta (15-30 Hz). Local neural synchrony was quantified by the relative spectral power of the canonical frequency bands within a given ROI. Long-range synchrony was computed using imaginary coherence, an established spectral coherence measure of neural synchrony that is robust to volume conduction effects[33]. To quantify information flow, phase transfer entropy (PTE) was also computed to assess the pair-wise directional interaction between ROI time courses[34], and directional information was computed using directional phase transfer entropy (dPTE)[35]. Data analysis was performed using the FieldTrip Matlab Toolbox[36] and custom made MATLAB code (version R2019a).

In addition, we utilized a linear, deterministic neural mass model (NMM)[37–40] to gain mechanistic insights on the relative balance of excitatory and inhibitory inputs based on the observed spectra. This NMM captures the local neural activity, as measured by the power spectral density (PSD) across each ROI and sleep-wake state. In this implementation of the NMM, whole-brain dynamics are deterministically modeled in closed form within the Fourier domain, using a canonical rate model that considers local cortical neural activity[37,38]. NMM methods are further described in Ranasinghe et al[41]. Specifically, we modeled a local signal as the summation of excitatory signals $x_e(t)$ and inhibitory signals $x_i(t)$ for every ROI, based on the Brainnetome parcellation[32]. Excitatory and inhibitory signals were modeled by a decay of the respective signals, feedback inputs from both excitatory and inhibitory signals, and noise. Parameters for the excitatory and inhibitory signals for individual regions included the neural gains for the excitatory, inhibitory, and alternating populations

represented by $g_{ee}$, $g_{ii}$, and $g_{ei}$, respectively; the characteristic time constants of excitatory and inhibitory populations represented by $\tau_e$ and $\tau_i$, respectively; the Gaussian white noise term represented by $p(t)$; and the Gamma-shaped ensemble neural impulse response, represented by $f_e(t)$ and $f_i(t)$ for inhibitory and excitatory contributions, respectively. The dynamics of the excitatory and the inhibitory signals are thus represented by the following:

$$\frac{\mathrm{d}x_e(t)}{\mathrm{d}t} = -\frac{f_e(t)}{\tau_e} \star \left(g_{ee}x_e(t) - g_{ei}f_i(t) \star x_i(t)\right) + p(t) \qquad 1$$

$$\frac{\mathrm{d}x_i(t)}{\mathrm{d}t} = -\frac{f_i(t)}{\tau_i} \star \left(g_{ii}x_i(t) + g_{ei}f_e(t) \star x_e(t)\right) + p(t) \qquad 2$$

For each ROI of the Brainnetome atlas, $g_{ee}$, $g_{ii}$, $\tau_e$, and $\tau_i$ were estimated, while $g_{ei}$ was fixed at 1. Optimization of the model was based on mean squared errors (MSE) between the actual and modeled PSD curve, for each ROI, participant, and sleep-wake state. The closed-form expression of the modeled PSD is described further in the Supplementary Methods. The minimization of the MSE for parameter optimization was performed using the basin hopping global optimization algorithm (Python)[42]. An empirical cumulative distribution function was constructed on the basis of MSE across all regions of interest, sleep-wake states, and patients; outliers were determined based on the threshold inclusion of 75% of the cumulative distribution (corresponding to MSE 37.6). Subsequent statistical testing to compare model parameters across sleep-wake states was performed using a repeated mixed models approach on a modular ROI level, accounting for subject, ROI, frequency, and state.

*Group statistics*

For statistical comparisons across states, the 210 cortical regional parcellation level spatial maps of the Brainnetome atlas were hierarchically configured to 44 modular level parcellation maps, giving rise to 990 functional connections, which includes the averaged measure (e.g. imaginary coherence) within each module. Linear mixed effects models with repeated measures were performed to identify statistically significant differences across two states for modules and modular connections. Statistics

were corrected for multiple comparisons (false discovery rate, FDR, level 0.05). Seed-based studies were additionally conducted to determine FC across select regions, including the default mode network and precuneus/posterior cingulate, as determined by atlas-based network definitions[43], following module-level extraction.

## RESULTS

*Local neural synchrony across sleep states*

Local neural synchrony, as measured by the spectral power, was averaged across all parcellations and revealed an expected alpha peak during wakefulness and a shift toward delta frequencies with transition to N1 and N2 (Fig. 1A). Source reconstructions of the mean relative spectral power demonstrated increased delta power predominantly over the bilateral prefrontal cortices with transition from wake to NREM (Fig. 1B). The anterior-posterior gradient in the alpha frequency band, as well as the central beta power, attenuated with transition from wake to light NREM (Fig. 2s). The spectral reconstructions are consistent with prior findings[44] and demonstrate the accurate acquisition of sleep-wake states.

*Long-range neural synchrony maps across sleep states*

Spatial maps of FC across classical frequency bands revealed frequency-specific patterns of long-range neural synchrony in light sleep as compared to wakefulness. Given the prominent shift to delta/theta frequencies with transition from wake to sleep (Fig. 1A), we focused on low frequency long-range neural synchrony patterns during sleep. Findings for other higher frequency bands are provided in the Supplementary Materials. Within the delta band, long-range synchrony, as measured by global FC, diffusely increased (Fig. 1C) with prominent long-range connections within and across bilateral frontal regions (i.e. SFG, MFG, PrG) and between frontal-parietal regions (i.e. between MFG, SFG and IPL, SPL; Figs. 1D, E).

Long-range synchrony increased from W to N1 (Fig. 1G; $t=19.4$, $p<0.001$) and W to N2 ($t=15.3$, $p<0.001$), and decreased from N1 to N2 ($t=-4.2$, $p<0.001$) in the delta band. This trend in long-range synchrony contrasts with that of local synchrony, in which the averaged local synchrony of N1 lies in magnitude in between W and N2 (Fig. 1F). The spatial maps of local and long-range synchrony had low correlation within N1 and W states and were not correlated within the N2 state (Fig. 1H; purple, green, and red lines; W, $R^2 = 0.054$, $p<0.001$; N1, $R^2 = 0.058$, $p<0.001$; N2, $R^2 = 0.003$, $p=0.433$,

respectively). On the other hand, there was a relatively high correlation *across* sleep-wakes states between local and long-range synchrony (Fig. 1H; black line, $R^2 = 0.586$, $p<0.001$). These findings suggest that the spatial maps of local synchrony do not strongly reflect the degree of long-range synchrony of individual regions with the transition to deeper stages of sleep.

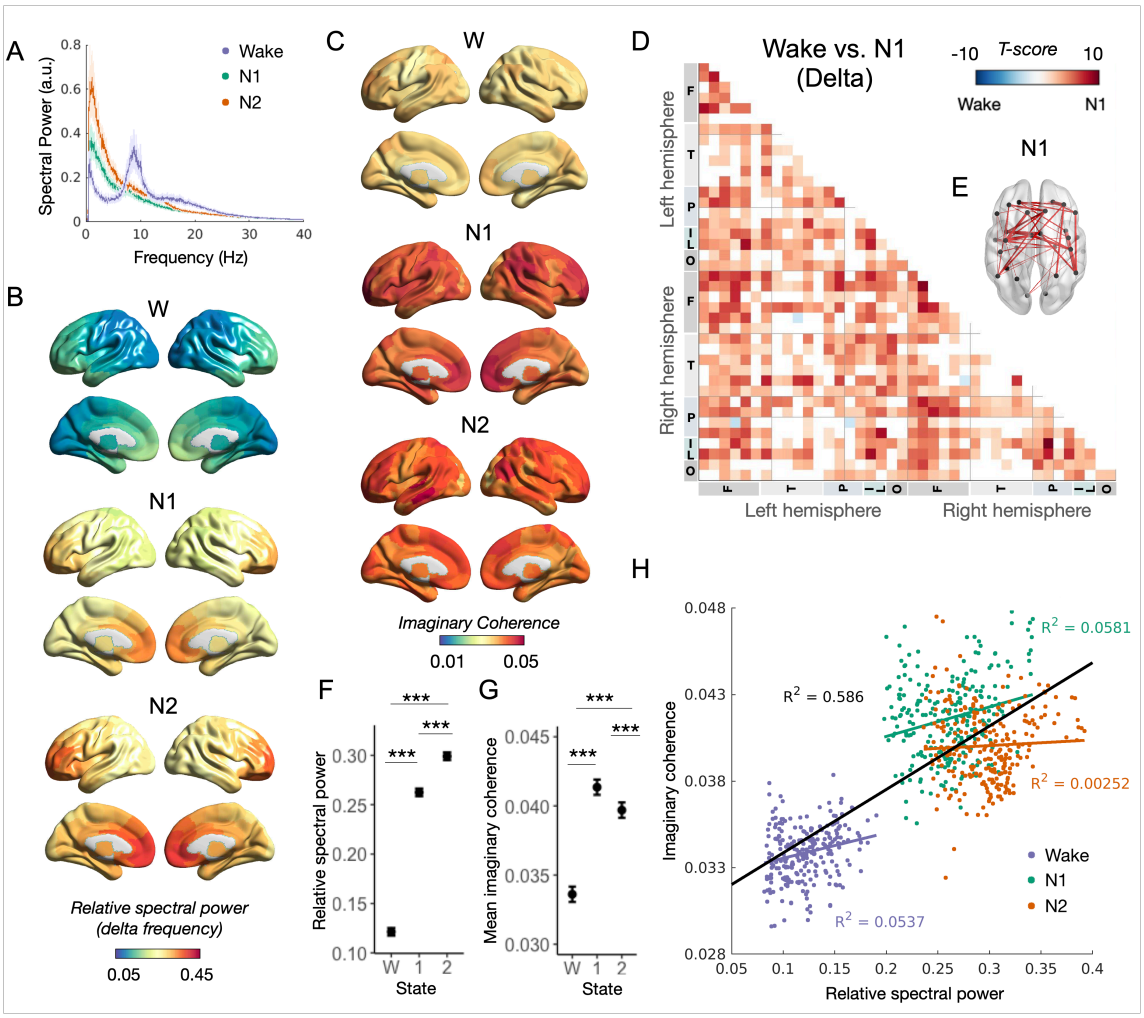


**Figure 1. Spectral and spatial FC maps between sleep-wake states in the delta frequency band.** A) Mean relative spectral power, averaged across regions and patients in wake (purple), N1 (green), and N2 (orange). Light shading represents the standard error across patients. B) Spatial maps of relative spectral power in sleep-wake states. C) Spatial map of global synchrony in W, N1, and N2 within the delta band, as measured by imaginary coherence. D) T-score map of differences in regional FC between W and N1 within the delta band. Lobar regions delineated on x- and y- axis

are further described in Table 1s. E) Top 50 highest positive functional connections, favoring N1. F) Mean relative spectral power of each sleep-wake state in the delta band, averaged across regions and patients. Error bars represent the 95% CI from the LS-mean. G) Mean long-range synchrony for each sleep-wake state in the delta band, averaged across region and patients. Error bars again denote 95% CI from the LS-mean. H) Association between averaged long-range synchrony (measured by mean imaginary coherence) and relative spectral power in the delta band. Each point represents an individual ROI within the spatial map. Linear regression and correlations of the averaged long-range synchrony and relative spectral power for individual ROIs are provided for within sleep-wake state and across state (black) populations.

Within the theta frequency band, bilateral frontal and occipital regions (i.e. IFG, MFG, ACC, and MVoCC, LOcC, and Pcun) exhibited increased connectivity, while bilateral temporal regions revealed reduced intra- and interhemispheric connectivity (i.e. STG, ITG, MTG, Hipp and Amy) in N1 as compared to W (Figs. 2A-C). Long-range synchrony again was observed to increase from W to N1 (Fig 2E, $t=7.55$, $p<0.001$) and to decrease from N1 to N2 ($t=-9.16$, $p<0.001$). Long-range synchrony was not statistically different between W and N2 ($t=-1.62$, $p=0.238$). Local and long-range synchrony measures again had low correlation within sleep states (Fig 2F; purple, green, and red; W, $R^2 = 0.204$, $p<0.001$; N1, $R^2 = 0.109$, $p<0.001$; N2, $R^2 = 0.098$, $p<0.001$, respectively), which increased in correlation when comparing across states (Fig 2F; $R^2 = 0.158$, $p<0.001$).

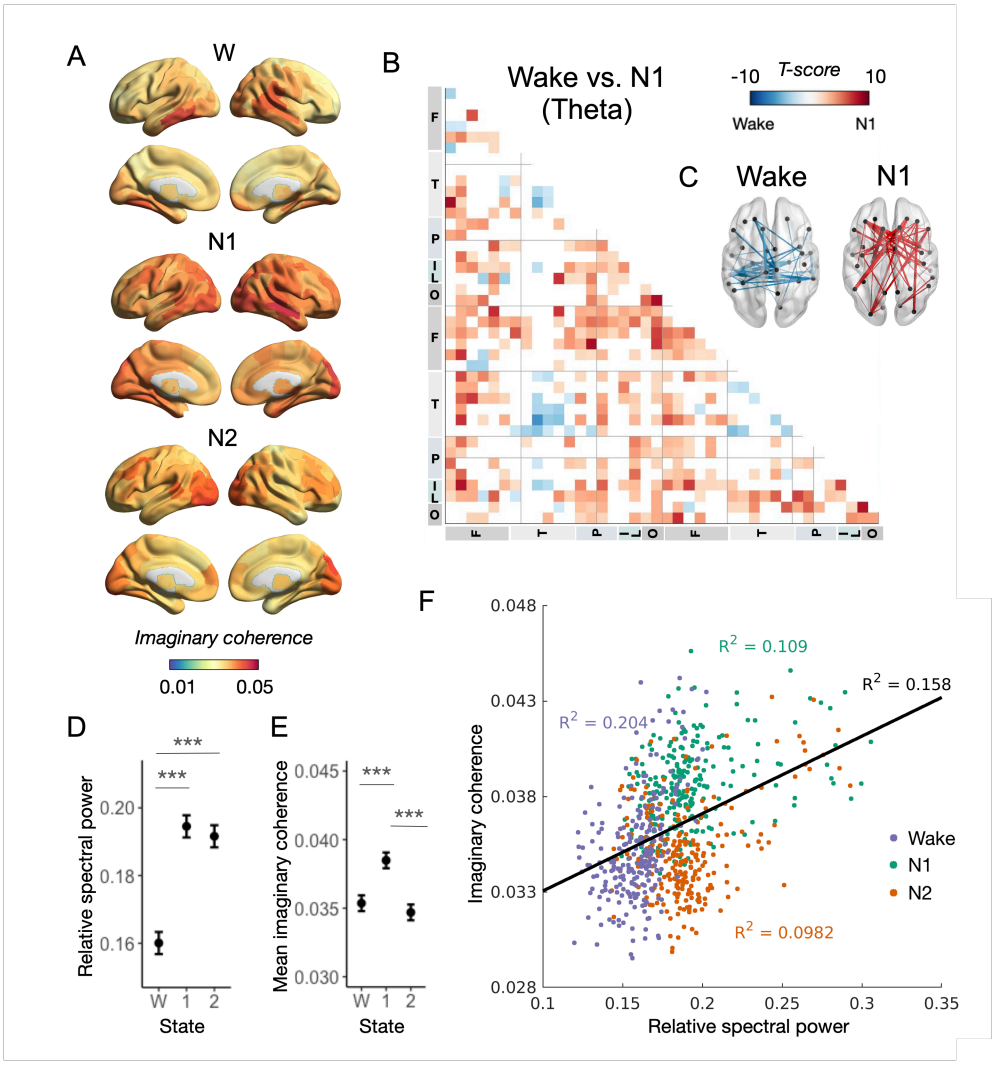


**Figure 2. Spatial FC maps between sleep-wake states in the theta frequency band.** A) Spatial map of global synchrony in W, N1, and N2 within the theta band, as measured by imaginary coherence. B) T-score map of differences in regional FC between W and N1 within the theta band. C) Top 50 highest positive and negative functional connections, favoring N1 (red) and W (blue), respectively. D) Mean relative spectral power of each sleep-wake state in the theta band, averaged across regions and patients. Error bars represent the 95% CI from the LS-mean. E) Mean long-range synchrony for each sleep-wake state in the theta band, averaged across region and patients. Error bars again denote 95% CI from the LS-mean. F) Association between the spatial maps of mean global FC and relative spectral power in the theta band.

Within the alpha frequency band, long-range synchrony increased over the bilateral frontal and temporal regions with relative sparing of the parietal-occipital region in N1, as compared to W (Fig. 3s). The beta band demonstrated relatively increased synchrony in interhemispheric connectivity and anterior temporal regions, during N1 as compared to W (Fig. 3s). The frequency-specific activation patterns in N1 and N2 were similar; however, N1 overall demonstrated an increase in long-range neural synchrony as compared to N2 (Fig. 4s).

*Default Mode Network (DMN) and PCC-Precuneus connectivity across sleep states*

Select seeded-analyses were performed on the DMN and PCC-Precuneus regions, as both local networks have been implicated in the transition to sleep, including in the mediation of conscious content[45–47]. Prior work has suggested that the anterior-posterior regions of the DMN remain coupled in light NREM[17,19] and then decouple in deep NREM[18,48–50]. Here, seeded analysis was performed to assess changes in neural synchrony between the anterior and posterior regions of the DMN across sleep-wake states (Fig. 3A). Frequency specific coupling between anterior and posterior regions of the DMN was observed with an increase in coupling in the delta band upon transition from W to N1 (Fig 3B; $t=7.762$, $p<0.001$) and a reduction from N1 to N2 ($t=-2.869$, $p=0.012$). Regional coupling within the anterior DMN was overall higher than within the posterior DMN in the delta band (Fig. 3B), consistent with the large-scale unseeded findings. In the alpha band, a trend of reduced anterior-posterior coupling from W to N1 (Fig. 3C; $t=-2.70$, $p=0.0192$) and increased coupling from N1 to N2 ($t=-2.69$, $p=0.0195$) was observed, but not statistically significant following multiple comparison corrections. These findings suggest that there is a spectral shift from alpha to delta frequencies in the coupling between anterior-posterior DMN during the transition from wake to light NREM and that the anterior-posterior DMN coupling has a unique pattern across sleep-wake states as compared to regional-level synchrony.

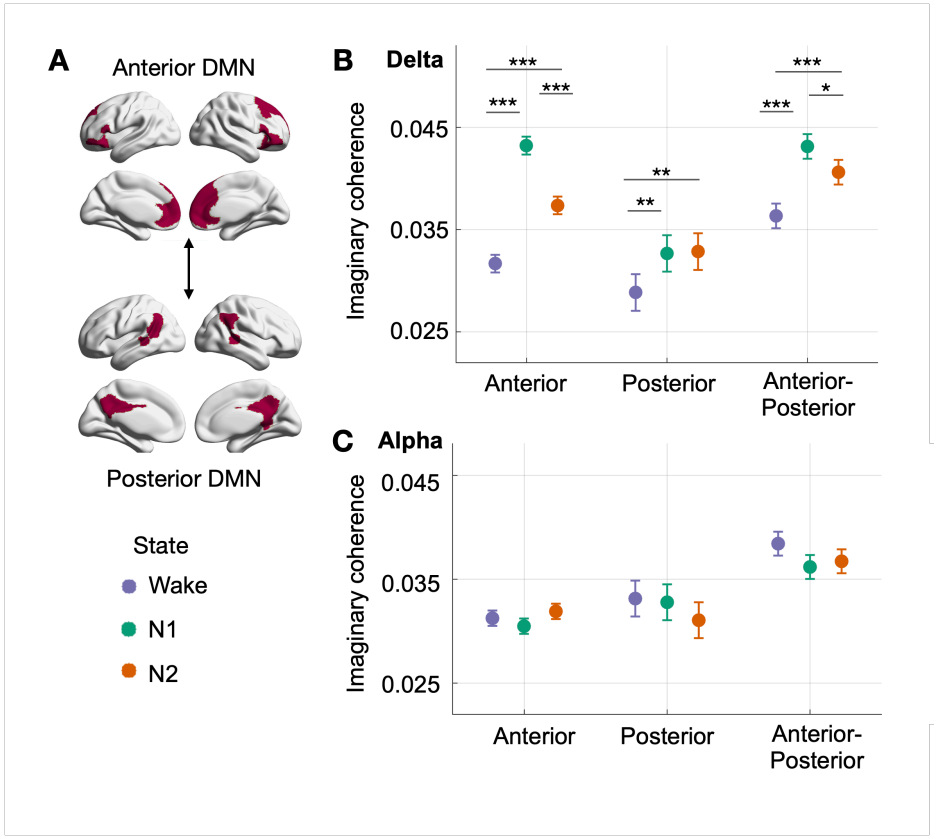


**Figure 3. Seeded study evaluating the FC between anterior and posterior regions of the DMN**. A) Voxels (red) that are involved and the anterior (*top*) and posterior (*bottom*) DMN. The anterior-posterior coupling as indicated by the arrows evaluates the interactions between anterior DMN voxels and posterior DMN voxels. B) Intrinsic FC within the anterior (*left*) and posterior (*middle*) DMN, and anterior-posterior coupling of the DMN (*right)* within the delta band and C) alpha band. Significance testing performed on multiple comparison testing across all regions (FDR level 0.5).

In addition, seeded analysis revealed distinct patterns of coupling intrinsic to the PCC-precuneus and between the PCC-precuneus and residual cortex (Fig. 4). While the coupling between the PCC-precuneus and the remainder of the brain largely reflected the patterns of global FC in delta and theta bands (Figs. 1H, 2F), the coupling within the PCC-precuneus was distinct. Notably, the intrinsic delta coupling within the PCC-precuneus during N1 was most similar to that of the wake state; in contrast, the coupling between the PCC-precuneus and the residual cortex during N1 was most

similar to N2. In addition, a statistically significant peak in the sigma band was identified in the cross-region couplings, but not in the intrinsic coupling within the PCC-precuneus.

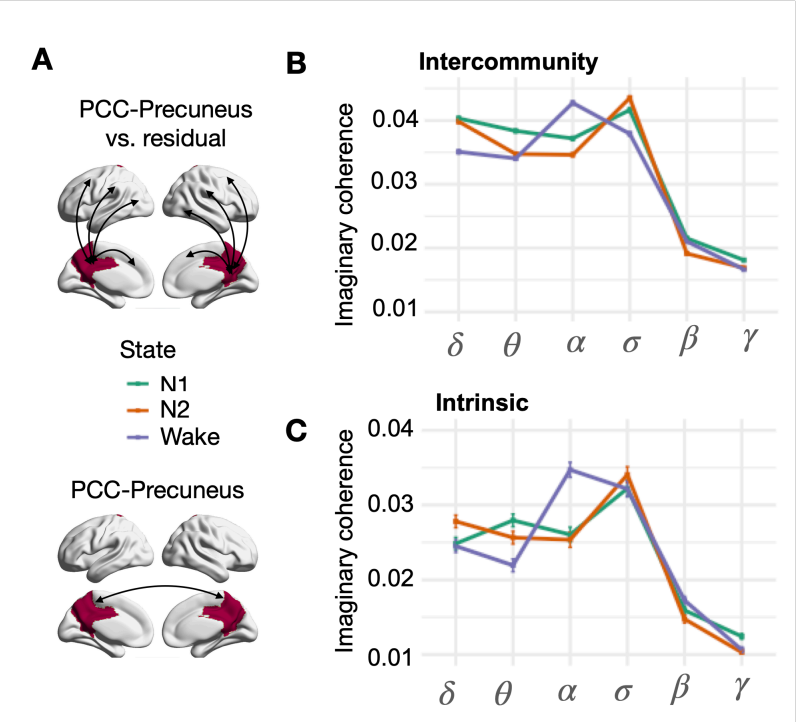


**Figure 4. Seeded study evaluating the FC between the PCC-precuneus and residual cortical structures (intercommunity) and within the PCC-precuneus (intrinsic)**. A) Voxels (red) that are involved in the PCC-precuneus with arrows indicating intercommunity (*top*) and intrinsic connectivity (*bottom*). B) FC relative to frequency bands for intercommunity and C) intrinsic connectivity.

*Information flow across sleep-wake states*

Information flow, as measured by dPTE, provides insight on the regional inputs and outputs that may influence local activity and synchronization. Within the delta band, aggregated inflow tracts targeting bilateral frontal regions increased in magnitude when transitioning from W to N1 and from N1 to N2 (Fig. 5). Outflow from the bilateral occipital cortices (e.g. bilateral occipital polar cortex, lingual gyrus, inferior occipital gyrus, middle occipital gyrus, and ventromedial parietooccipital sulcus) were largely directed to the orbital frontal cortices during wakefulness and to bilateral frontal regions more broadly during N1. Strikingly, with transition to N2, the outflow from the posterior regions gave rise to primary

inputs not only to bilateral frontal regions, but also to the bilateral temporal lobe, insula, and cingulate (Figs. 5C, F). In turn, indirect outflow regions (i.e. bilateral temporal lobe, insula, and cingulate) then provided inflow into the bilateral frontal region (Fig. 5C), representing a hierarchical organization of information flow that converges on the bilateral frontal regions. In comparison to W, N1 and N2 demonstrated increased information flow across broad cortical regions both directly and indirectly into the bilateral frontal region (Fig 5G, H), suggesting that the prominent anterior delta power seen at sleep onset is enabled through the inputs of broadly distributed and hierarchically organized cortical activity.

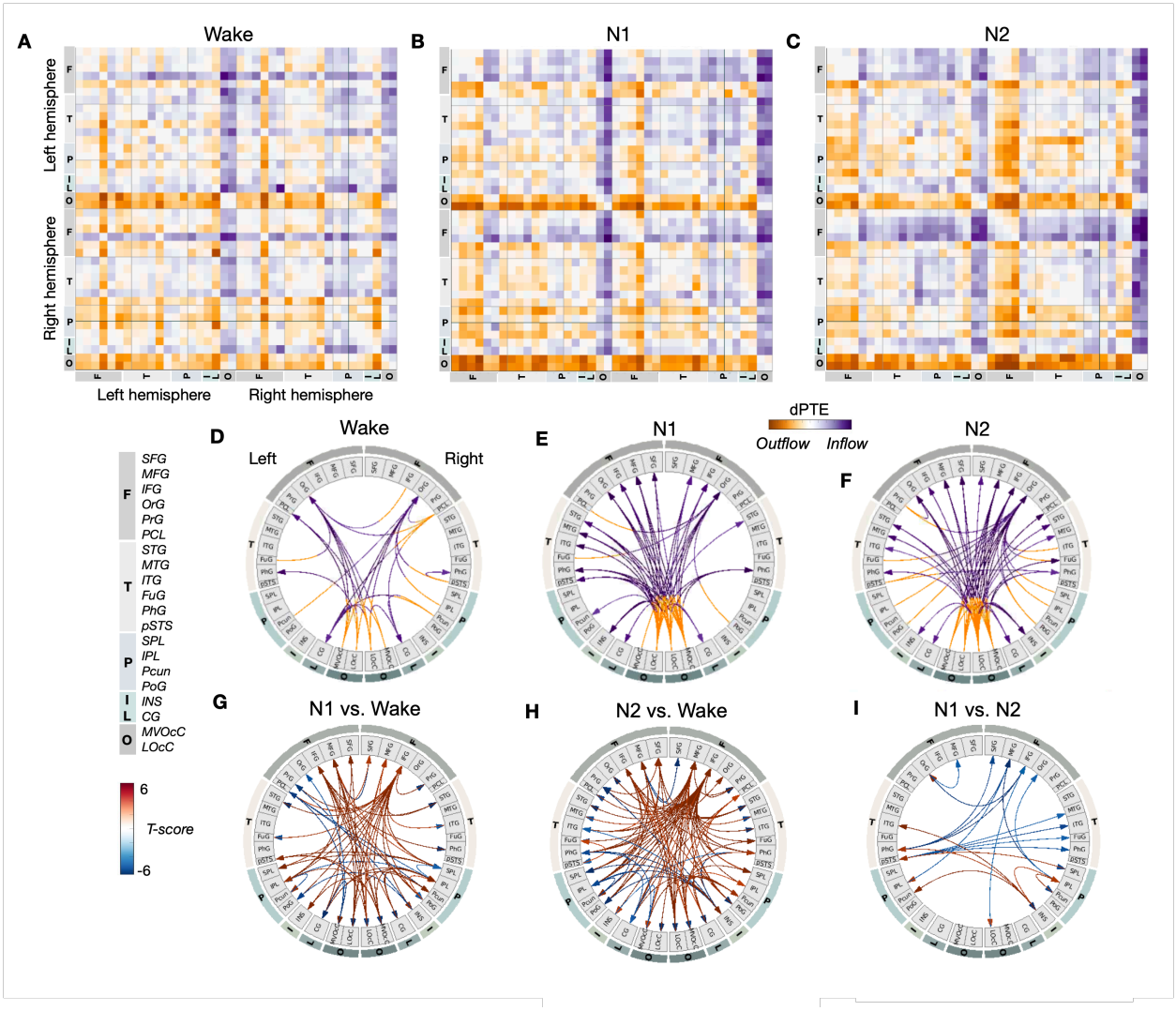


**Figure 5. Directed information flow of sleep-wake states in the delta frequency band.** A-C) Directed FC as measured by directional phase transfer entropy (dPTE) across W, N1, and N2. From

W to N1 and N2, there is increasing magnitude of dPTE with an aggregative inflow into the bilateral frontal regions. D-F) Alternate visualization of directed FC colored by orange (outflow) and purple arrow (inflow). The visualization across W, N1, and N2 using a common threshold for depicting increased magnitudes and trajectories of the directed FC. G-I) T-scores plotted indicating magnitude changes between specified states (accounting for FDR level 0.5)

In the alpha frequency band, there was an overall reduction in the occipital-frontal information flow (Fig. 5s) with transition from wake to NREM. In addition, the strong outflow tracks seen from the precuneus and IPL attenuated with the transition from W to N1 and from N1 to N2 (Fig. 5s). Importantly, these findings suggest that with the transition to sleep, the posterior-anterior information flow does not cease, but rather that there is a spectral shift to lower frequencies.

*Neural mass modeling reveals cortical excitation and inhibition balance changes in sleep states*

Finally, the balance between cortical excitation and inhibition was examined by modeling estimated regional spectral power using a deterministic NMM that captures local oscillatory dynamics (Fig 6A). The two indices of the NMM that were optimized to fit local electrophysiology included the characteristic time constants ($\tau_e, \tau_i$), representing the time-course of the underlying inhibitory and excitatory drive, and the gain ($g_{ee}, g_{ii}$), representing the strength of recurrent local circuits. From wake to light NREM, both the $g_{ee}/g_{ii}$ and the $\tau_e/\ \tau_i$ ratio was observed to increase; differences between N1 to N2 were not statistically significant (Fig. 6B). The resultant excitation-to-inhibition model neural ensemble ratio ($X_e/X_i$) revealed an increase in the excitation-to-inhibition balance from wake to light NREM (N1-W, t=10.4, p<0.001; N2-W, t=8.2, p<0.001) and a trend toward decreasing magnitudes from N1 to N2, although non-significant (N1-N2, t=2.3, p = 0.052; Fig 6C). These findings suggest that the transitional period to sleep may comprise a complex excitation-to-inhibition balance, in which *local* excitability-to-inhibition increases with the transition to NREM.

By modeling local dynamics, the excitation-to-inhibition ratio was furthermore demonstrated to be heterogeneous across the cortical surface within sleep-wake states (Fig 6D). The cortical excitation-to-inhibition ratio was highest over the bilateral frontal lobes during N1, while relatively reduced during wakefulness (Fig 6E). Furthermore, the bilateral parietal regions exhibited relatively increased cortical excitation-to-inhibition during wakefulness, as compared to light NREM (Fig. 6E). Comparison of the raw spectra to the model spectra (Fig. 6F) revealed overall similarity in the profile of the spectra and peak frequencies. As homeostatic regulation during sleep has been thought be achieved through tuning of the synaptic strengths of excitatory and inhibitory circuits to augment the excitation-to-inhibition balance, our computational modeling using NMM illustrates that the local cortical dynamics identified during sleep onset ultimately yields a spatially heterogeneous homeostatic cortical process at the sleep transition.

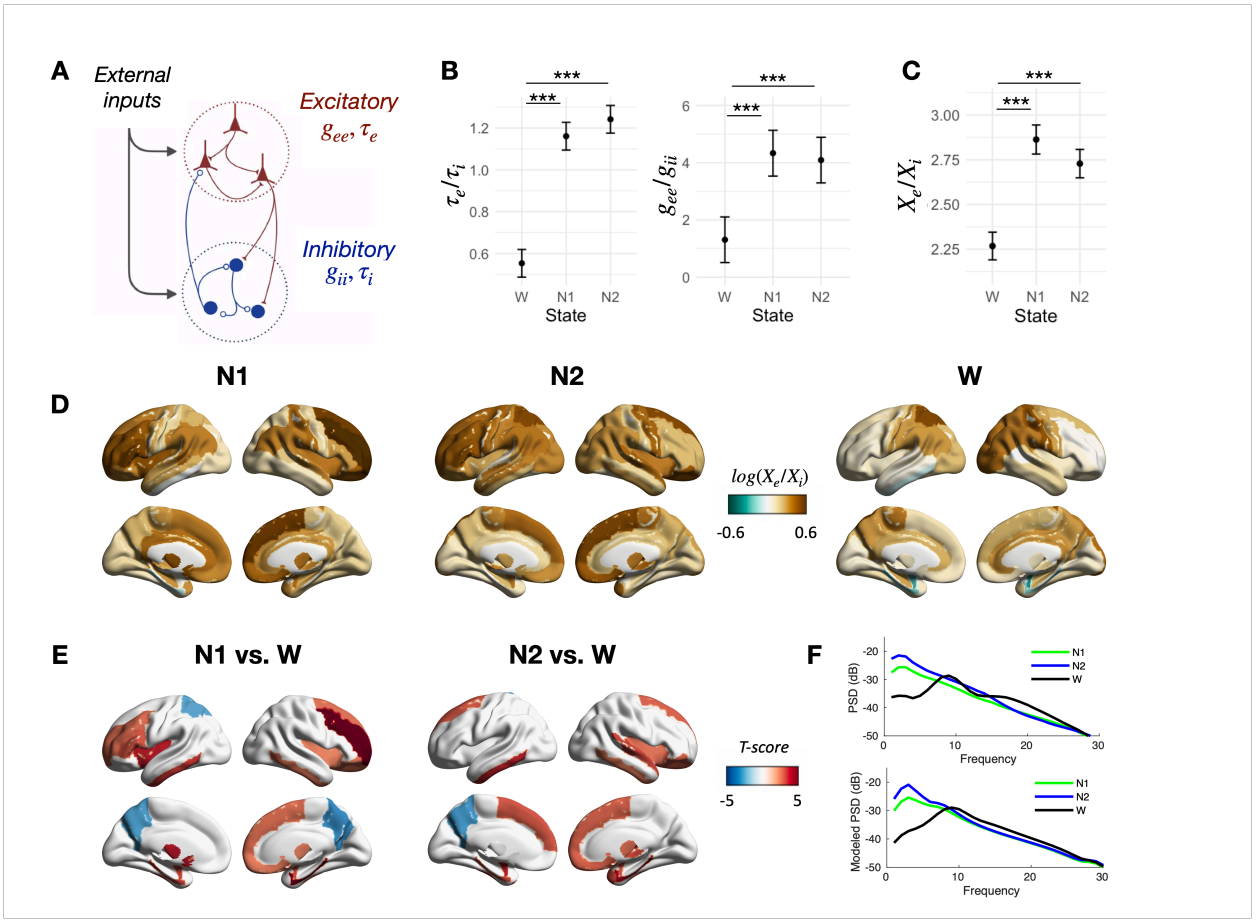

**Figure 6. Biophysical NMM model across sleep-wake states demonstrated reduced excitation-inhibition with transition to sleep.** A) Depiction of NMM, comprised of both excitatory and inhibitory inputs and modeled with time constants ($\tau$) and gain ($g$) parameters. B) Optimized parameters of $\tau_e/\ \tau_i$ and $g_{ee}/g_{ii}$ across sleep-wake states. C) Excitatory-inhibitory ratios ($X_e/X_i$) across sleep-wake states, revealing an increased excitation-to-inhibition with transition from wake to sleep. D) Spatial maps of $X_e/X_i$ across sleep-wake states, revealing cortical heterogeneity in excitability. E) T-scores reflecting differences between N1 vs. W (*left*) and N2 vs. W (*right*) across different ROIs. Depicted T-scores are thresholded to account for multiple comparison testing (FDR level 0.05). F) Actual (*top*) and modeled (*bottom*) power spectral density curves across sleep-wake states.

## DISCUSSION

The characterization of whole-brain neural oscillations is essential to advancing our understanding of distributed network interactions underlying the transition to sleep. Descriptions of large-scale brain networks have relied chiefly on fMRI/PET imaging, which lack the temporal resolution and access to electrophysiology, and on EEG, which has limited spatial coverage and sensor level analysis. By using MEG imaging, a whole-brain, high-density imaging methodology, to simultaneously evaluate spectral power, functional connectivity, and information flow, we identify local and long-range cortical structure that underlie the transition from waking to NREM sleep. Our findings reveal that the transition to sleep is accompanied by specific cortical patterns of neural synchrony that are coordinated in frequency and spatial extent (e.g. local, long-range, and network based). Furthermore, the underlying organization of neural oscillations reveals a multilevel hierarchical flow of information, in which there are both direct and indirect inputs of information flow to the bilateral frontal regions that arise from broad cortical regions. Finally, by deploying a NMM optimized to the measured local electrophysiology, we demonstrate spatially heterogeneous excitatory-to-inhibitory contributions upon the transition to sleep, suggestive of local homeostatic processes. As a simultaneous evaluation of local and long-range synchrony and information flow has not yet been performed, we review the literature in each of these domains in the context of our findings and then elaborate on how our NMM modeling fits in with experimental techniques.

Studies from the past decade have revealed that sleep onset is not a homogenous process[3,51–54]. Seminal PET studies provided the initial evidence of differential deactivation of cortical association regions with transition from waking to NREM, including in the prefrontal cortex, anterior cingulate, precuneus and mesial temporal structures, in addition to the deactivation of subcortical structures[55,56]. Slow wave activity using EEG/MEG has been identified to originate in anterior medial regions[51,57], later involving parietal, temporal and occipital regions in an anterior to posterior direction[51]. The onset of slow wave activity coincides with an early rise in delta power in the frontal regions[25,27,57] and an increase in theta synchrony in the occipital region[52,57]. These findings are

similarly recapitulated in our data (Figs. 1B), in which the spectral reconstructions representing local synchrony revealed prominent mesial frontal delta. Across all frequency groups, the correlations between the spatial maps of spectral power and global synchrony were significantly correlated although with low correlational values (e.g. Figs. 1H, 2F), indicating that local oscillatory activity did not strongly reflect the aggregation of long-range interactions. Similar findings in rest-state between relative power and mean PLI have been previously identified[58], suggesting the need to simultaneously evaluate both local and long-range synchrony measures.

Large-scale functional connectivity studies using fMRI[20,21,24] and MEG[28] have demonstrated widespread increases in long-range synchrony from W to N1 and N1 to N2, and a subsequent breakdown in long-range synchrony with transition to N3[20,21,59]. The widespread, homogenous synchronization across large spatial distances has been associated with decreased global integration[60], theorized to account for loss of consciousness. The suggestion of a corticocortical synchronization process, complementing the “bottom-up” ascending arousal system[51], raises the possibility of coordinated long-range cortical oscillations. In contrast to prior studies, our findings demonstrate that long-range interactions were evident during light NREM with predominant bifrontal and fronto-parietal interactions in the delta band (Figs. 1D, E), and fronto-occipital and fronto-parietal interactions in the theta band (Figs. 2B, C). Importantly, prior work with MEG[28] revealing widespread increases in coherence have been limited by sensor-based FC mappings, which suffers from overlapping lead fields and spurious connectivity and may conceal underlying structure. Furthermore, fMRI connectivity studies are limited by its temporal resolution. Our findings ultimately reveal the orchestration of not only local but also intrinsic long-range subnetworks of regions across multiple frequency bands (Figs. 1C-F, 2A-D), complementing the host of other circuit-specific oscillations of NREM[61]. Our findings additionally confirm prior studies[20,21,28,62] reporting that the overall connectivity in N1 is increased as compared to in W and N2 in the delta band. In contrast, spectral power demonstrates a monotonic increase from W to N1 and N1 to N2. These findings suggest that N1 composes a unique state that is not a transitional or ill-defined state between wake

and sleep, which has previously been suggested due to the relatively low interrater reliability of identifying N1 based on less well-defined PSG features[63] and challenges of machine learning fMRI studies to extract unique N1 states[21,64,65]. Rather, its distinctly elevated global long-range synchrony speaks to the complexity of the N1 state, which has been characterized by unique behavioral observations, including sleep mentation, responsiveness to sensory stimuli, or lucid dreaming[4,66,67].

Complementing the evaluation of local and long-range synchrony across regions, we also assessed the directionality of regional interactions, as measured by information flow. Previously, dominant posterior to anterior patterns of information flow of alpha frequencies have been identified during resting state[68]. Our findings confirm the posterior to anterior patterns of information flow during resting state for higher frequencies (Fig. 4s), and furthermore newly demonstrate increasing organization and magnitude of information flow in the delta frequency band with transition from wake to light NREM. The findings of a dominant posterior to anterior pattern of information flow (i.e. from parietal-occipital regions to frontal regions), in addition to indirect information flow (i.e. from posterior regions to bilateral temporal regions, which secondarily flow to the bilateral frontal lobes; Figs. 5C, F) in the delta frequency band during light NREM, demonstrate multilayer circuitry of neural information flow or sequence of assemblies[61,68,69]. In contrast to prior EEG-based studies revealing an inversion of directionality from occipital-to-frontal to frontal-to-occipital during sleep onset[26,70,71], our findings suggest a spectral shift in the prominent organizational pattern, while maintaining the posterior-to-anterior information flow. In addition to the increased number of sensors for source reconstruction approaches, MEG provides a reference free methodology for computing information flow, thereby preventing the potential bias associated with referenced based methods such as EEG.

Interestingly, our work does qualitatively suggest a broad hemispheric difference in FC across different frequency bands (Fig 6s). Prior work has demonstrated the presence of frequency-specific interhemispheric information flow with sleep onset[72]. Future larger-sample studies would be of great

interest to assess how the laterality of hemispheric FC relates to language lateralization and dominance.

In addition to large-scale, unseeded analyses, we performed seeded analyses on key resting-state targets. The DMN has garnered significant interest over the last two decades due to its robust activation during resting state and deactivation with externally mediated attention and tasks[45,73]. As such, the DMN has been thought to play a role in internally mediated cognitive processing and self-referential behavior[45], reflecting or arguably mediating a critical component of conscious content[47,50]. PET/fMRI studies have identified that the intrinsic coupling of the DMN remains intact with light NREM[17,19] and REM[50], while the anterior and posterior regions of the DMN decouple in deep NREM[18,48–50]. To complement these studies, our findings probing the intrinsic coupling between anterior-posterior regions of the DMN reveal frequency specificity with transition to light NREM. In contrast to EEG-based studies that have revealed anterior-posterior decoupling at sleep onset[49,70], we identified that the anterior-posterior connectivity exhibits a spectral shift from higher to lower frequencies with transition to light NREM (Fig 3). As PET/fMRI power modulation has previously been associated with ultraslow amplitude modulation of higher frequency neural oscillations, including beta[74], gamma[75], or multiple frequency bands[22,76,77], shifts to lower frequency bands may not be captured with these imaging modalities. Future work to probe deeper stages of sleep would be of great interest.

Within the DMN, the PCC/precuneus has been implicated as a low frequency synchronizer[49] and central hub involved in conscious processing with the external environment[46,78,79] and conscious self-awareness[46,80,81]. The connectivity between the PCC/precuneus and the remainder of the cortex is demonstrated here to be distinct from the intrinsic coupling within the region. Specifically, within the delta frequency band, the intrinsic coupling within the PCC/precuneus during N1 was most consistent with that of wakefulness (Fig. 4B), whereas the interactions between the PCC and the residual cortex mimicked the trends seen with averaged long-range synchrony. This finding suggests

that the intrinsic connectivity within the PCC/precuneus, particularly in the delta frequency band, has a delayed increase, occurring at N2 rather than to N1, as compared to the connectivity between PCC/precuneus and the residual cortex. This finding may reflect the concept that self-reflective activity reduces gradually, rather than acutely, with progression to deeper stages of sleep[16,18].

Finally, we investigated whether the identified neural oscillatory patterns may give rise to a spatial heterogeneity in the degree of cortical excitation-to-inhibition. Cortical excitability has been demonstrated to increase with time awake or sleep deprivation[82,83] and decrease during sleep and the circadian cycle[83–85], as measured by neuronal firing rates, synchronization, and propagation of transcranial magnetic stimulation (TMS)[83,86]. In our study, by utilizing a NMM to model the cortical excitation-to-inhibition balance, we demonstrated that the observed physiology yields a global increase in *local* cortical excitation-to-inhibition activity with the transition from wake to light NREM, consistent with prior methods using TMS[87]. Specifically, prior TMS findings revealed an enhancement of early or local TMS-EEG responses during sleep, followed by a global attenuation reflecting an overall global breakdown in effective cortical connectivity[87]. The amplified early TMS-EEG response, which has also been observed with visual, auditory and sensory stimulation[88], supports the conception of increased *local* excitation-to-inhibition during NREM and has been hypothesized to relate to an increased drive of post-synaptic excitatory neurons or a reduction in synaptic depression, synchronization of local cortical populations or activation of thalamocortical circuits[87,89,90].

By employing local NMM modeling and leveraging whole-brain local field potential, cortical spatial maps of excitation-to-inhibition can be fully elaborated, in contrast to seeded processes, e.g. TMS impulses[83,86,91,92], magnetic resonance spectroscopy[93], or direct measurements of excitatory and inhibitory neurotransmitters[94,95]. As such, we further demonstrate for the first time that the degree of excitation-to-inhibition across the cortex is non-uniform (Fig. 6D, E). We identify that the primary increase in local excitation-to-inhibition occurs in the bilateral frontal lobes during light NREM, which

is largely decreased during wakefulness. Meanwhile, the greatest local excitation-to-inhibition is within the parietal-occipital regions during wakefulness. Our findings reinforce the conception that sleep is composed of spatially heterogeneous network dynamics that furthermore reflect complex homeostatic patterns within the cortex.

This work has limitations, including the quality of sleep captured and the relatively modest sample size. Due to the noisy environment and time-limitations of a recording session within the MEG scanner, the sleep quality in the healthy participants was at times fragmented. In addition, deep NREM stages were not obtained across all patients and thus not included in the analysis. To address the sleep fragmentation, shortened epochs of 15s were utilized and concatenated together to formulate the most faithful representations of sleep-wake states. Future efforts may benefit from overnight or sleep-deprived recording sessions to obtain longer, continuous periods of sleep-wake states. In addition, this study incorporates a modest sample size of fourteen patients, who are also older in age. A future research direction includes the characterization of differences in neural synchrony patterns during sleep across age. Although MEG imaging offers improved spatial resolution as compared to other EEG modalities, source reconstruction methodologies, including adaptive beamformers[31], are still an active area of research with respect to modeling spontaneous neural activity; thus as compared to other modalities (e.g. fMRI and intracranial EEG), there are trade-offs with respect to high spatial resolution and acquiring electrophysiology or whole-brain coverage. Finally, although the linear NMM captures the frequency spectra directly through a closed form solution, the primary limitations of the NMM employed in this study include its inability to capture non-linear complexities of the brain.

In summary, our work identifies cortical oscillations structured across space on multiple scales (i.e. local, long-range, and network) and hierarchically organized across time (e.g. frequency-specific interactions) with the transition to NREM sleep. Multilayer information flow from broad cortical regions are directed to the mesial frontal regions in the delta frequency, contributing to the

synchronization of local oscillations. Finally, the captured electrophysiology supports a spatially heterogeneous increase of cortical excitability relative to inhibition with transition to sleep. Together, our findings suggest that the transition to sleep is accompanied by coordinated, frequency and spatially (e.g. local, long-range, and network based) specific cortical patterns of activity suggestive of hierarchically structured corticocortical interactions, which complement bottom-up sleep-onset mechanisms modulated at the subcortical and brainstem level. These findings may ultimately explain pathologic phenomena, including why the propensity of seizure activity is spatially heterogeneous across the cortex in NREM[96,97].

**Acknowledgments**

We thank our subjects for volunteering to participate in the study.

**Data Availability**

The data that support the findings of this study are available from the corresponding author upon reasonable request.

**Author Contributions**

J.M.F., K.K., P.V., K.G.R., H.E.K., A.R., A.D.K., and S.S.N. contributed to the conception of the work, analysis, and interpretation of the data. H.M. contributed to the analysis of the data. A.M.F., K.G.R., and K.V. contributed to the acquisition of the data. J.M.F., P.V., A.D.K., S.S.N. contributed to the writing of the manuscript. All authors have reviewed and approved the submitted manuscript.

**Funding:**

Research reported in this publication was supported by the NIH grants 5TL1TR001871-05 (JMF), R01EB022717 (SSN), R01NS100440 (SSN), R01AG062196 (SSN), DOD CDMRP Grant W81XWH1810741 (SSN), UCOP-MRP-17-454755 (SSN), K08AG058749 (KGR), K23 AG038357 (KAV); a grant from John Douglas French Alzheimer's Foundation (KV); grants from Larry L. Hillblom Foundation: 2015-A-034-FEL and (KGR); 2019-A-013-SUP (KGR); a grant from the Alzheimer's Association: (PCTRB-13-288476) (KV), and made possible by Part the CloudTM, (ETAC-09-133596); S. D. Bechtel, Jr Foundation (KV), and a research contract from Ricoh MEG USA Inc. (SSN, HEK). Its contents are solely the responsibility of the authors and do not necessarily represent the official views of sponsoring agencies.

**Abbreviations:** Amy = amygdala; CG = cingulate gyrus; FC = functional connectivity; FuG = fusiform gyrus; Hipp = hippocampus; IFG = inferior frontal gyrus; IPL = inferior parietal lobule; INS = insula; ITG = inferior temporal gyrus; IQR = interquartile range; LOcC = lateral occipital cortex; MEG

= magnetoencephalography; MFG = middle frontal gyrus; MTG = middle temporal gyrus; MVOcC = medioventral occipital cortex; NREM = non-rapid eye movement; N1 = stage 1 sleep (NREM); N2 = stage 2 sleep (NREM); OrG = orbital frontal gyrus; PCL = paracentral lobule; Pcun = precuneus; PhG = parahippocampal gyrus; PoG = postcentral gyrus; PrG = precentral gyrus; pSTS = posterior superior temporal sulcus; ROI = region of interest; SFG = superior frontal gyrus; SPL = superior parietal lobule; STG = superior temporal gyrus; W = wake

## References


1. Brown RE, Basheer R, McKenna JT, Strecker RE, McCarley RW. CONTROL OF SLEEP AND WAKEFULNESS. *Physiol Rev*. 2012;92(3):1087. doi:10.1152/PHYSREV.00032.2011
2. Saper CB, Fuller PM. Wake-Sleep Circuitry: An Overview. *Curr Opin Neurobiol*. 2017;44:186. doi:10.1016/J.CONB.2017.03.021
3. Bernardi G, Siclari F, Handjaras G, Riedner BA, Tononi G. Local and Widespread Slow Waves in Stable NREM Sleep: Evidence for Distinct Regulation Mechanisms. *Front Hum Neurosci*. 2018;12:248. doi:10.3389/fnhum.2018.00248
4. Siclari F, Tononi G. Local aspects of sleep and wakefulness. *Curr Opin Neurobiol*. 2017;44:222-227. doi:10.1016/j.conb.2017.05.008
5. Huber R, Ghilardi MF, Massimini M, Tononi G. Local sleep and learning. *Nature*. 2004;430(6995):78-81. doi:10.1038/nature02663
6. Kringelbach ML, Deco G. Brain States and Transitions: Insights from Computational Neuroscience. *Cell Rep*. 2020;32(10):108128. doi:10.1016/j.celrep.2020.108128
7. M. Krueger J, Tononi G. Local Use-Dependent Sleep; Synthesis of the New Paradigm. *Curr Top Med Chem*. 2012;11(19):2490-2492. doi:10.2174/156802611797470330
8. Thomas CW, Guillaumin MCC, McKillop LE, Achermann P, Vyazovskiy V V. Global sleep homeostasis reflects temporally and spatially integrated local cortical neuronal activity. *Elife*. 2020;9:1-25. doi:10.7554/ELIFE.54148
9. Krone LB, Yamagata T, Blanco-Duque C, et al. A role for the cortex in sleep–wake regulation. *Nat Neurosci 2021 249*. 2021;24(9):1210-1215. doi:10.1038/s41593-021-00894-6
10. Helm E van der, Walker MP. Overnight Therapy? The Role of Sleep in Emotional Brain Processing. *Psychol Bull*. 2009;135(5):731. doi:10.1037/A0016570
11. R G, J C. The interplay between sleep and emotion regulation: conceptual framework empirical evidence and future directions. *Curr Psychiatry Rep*. 2014;16(11). doi:10.1007/S11920-014-0500-X
12. Palmer CA, Alfano CA. Sleep and emotion regulation: An organizing, integrative review. *Sleep Med Rev*. 2017;31:6-16. doi:10.1016/J.SMRV.2015.12.006

13. Diekelmann S, Born J. The memory function of sleep. *Nat Rev Neurosci 2010 112*. 2010;11(2):114-126. doi:10.1038/nrn2762

14. Klinzing JG, Niethard N, Born J. Mechanisms of systems memory consolidation during sleep. *Nat Neurosci 2019 2210*. 2019;22(10):1598-1610. doi:10.1038/s41593-019-0467-3

15. Stickgold R. INSIGHT REVIEW Sleep-dependent memory consolidation. 2005. doi:10.1038/nature04286

16. Hobson JA, Pace-Schott EF. The cognitive neuroscience of sleep: neuronal systems, consciousness and learning. *Nat Rev Neurosci 2002 39*. 2002;3(9):679-693. doi:10.1038/nrn915

17. Larson-Prior LJ, Zempel JM, Nolan TS, Prior FW, Snyder A, Raichle ME. Cortical network functional connectivity in the descent to sleep. *Proc Natl Acad Sci U S A*. 2009;106(11):4489-4494. doi:10.1073/pnas.0900924106

18. Horovitz SG, Braun AR, Carr WS, et al. Decoupling of the brain's default mode network during deep sleep. *Proc Natl Acad Sci U S A*. 2009;106(27):11376-11381. doi:10.1073/pnas.0901435106

19. Horovitz SG, Fukunaga M, De Zwart JA, et al. Low frequency BOLD fluctuations during resting wakefulness and light sleep: A simultaneous EEG-fMRI study. *Hum Brain Mapp*. 2008;29(6):671-682. doi:10.1002/hbm.20428

20. Spoormaker VI, Schröter MS, Gleiser PM, et al. Development of a large-scale functional brain network during human non-rapid eye movement sleep. *J Neurosci*. 2010;30(34):11379-11387. doi:10.1523/JNEUROSCI.2015-10.2010

21. Tagliazucchi E, Laufs H. Decoding Wakefulness Levels from Typical fMRI Resting-State Data Reveals Reliable Drifts between Wakefulness and Sleep. *Neuron*. 2014;82(3):695-708. doi:10.1016/j.neuron.2014.03.020

22. Liu Z, Fukunaga M, de Zwart JA, Duyn JH. Large-scale spontaneous fluctuations and correlations in brain electrical activity observed with magnetoencephalography. *Neuroimage*. 2010;51(1):102-111. doi:10.1016/j.neuroimage.2010.01.092

23. Spoormaker VI, Schröter MS, Gleiser PM, et al. Behavioral/Systems/Cognitive Development of a Large-Scale Functional Brain Network during Human Non-Rapid Eye Movement Sleep. 2010. doi:10.1523/JNEUROSCI.2015-10.2010

24. Spoormaker VI, Czisch M, Maquet P, Jäncke L. Large-scale functional brain networks in human non-rapid eye movement sleep: Insights from combined electroencephalographic/functional magnetic resonance imaging studies. *Philos Trans R Soc A Math Phys Eng Sci*. 2011;369(1952):3708-3729. doi:10.1098/rsta.2011.0078

25. Ioannides AA, Liu L, Poghosyan V, Kostopoulos GK. Using MEG to understand the progression of light sleep and the emergence and functional roles of spindles and K-complexes. *Front Hum Neurosci*. 2017;11:313. doi:10.3389/fnhum.2017.00313

26. L DG, F V, M F, G C, PM R, C B. Antero-posterior functional coupling at sleep onset: changes as a function of increased sleep pressure. *Brain Res Bull*. 2005;65(2):133-140. doi:10.1016/J.BRAINRESBULL.2004.12.004

27. L DG, M F, G C, R C. Antero-posterior EEG changes during the wakefulness-sleep transition. *Clin Neurophysiol*. 2001;112(10):1901-1911. doi:10.1016/S1388-2457(01)00649-6

28. Liu Z, Fukunaga M, de Zwart JA, Duyn JH. Large-scale spontaneous fluctuations and correlations in brain electrical activity observed with magnetoencephalography. *Neuroimage*. 2010;51(1):102-111. doi:10.1016/j.neuroimage.2010.01.092

29. Cai C, Xu J, Velmurugan J, et al. Evaluation of a dual signal subspace projection algorithm in magnetoencephalographic recordings from patients with intractable epilepsy and vagus nerve stimulators. *Neuroimage*. 2019;188:161-170. doi:10.1016/j.neuroimage.2018.11.025

30. Guggisberg AG, Honma SM, Findlay AM, et al. Mapping functional connectivity in patients with brain lesions. *Ann Neurol*. 2008;63(2):193-203. doi:10.1002/ana.21224

31. Sekihara K, Hild KE, Nagarajan SS. A novel adaptive beamformer for MEG source reconstruction effective when large background brain activities exist. *IEEE Trans Biomed Eng*. 2006;53(9):1755-1764. doi:10.1109/TBME.2006.878119

32. Fan L, Li H, Zhuo J, et al. The Human Brainnetome Atlas: A New Brain Atlas Based on Connectional Architecture. *Cereb Cortex*. 2016;26(8):3508-3526. doi:10.1093/cercor/bhw157

33. Sanchez Bornot JM, Wong-Lin KF, Ahmad AL, Prasad G. Robust EEG/MEG Based Functional Connectivity with the Envelope of the Imaginary Coherence: Sensor Space Analysis. *Brain Topogr*. 2018;31(6):895-916. doi:10.1007/s10548-018-0640-0

34. Lobier M, Siebenhühner F, Palva S, Palva JM. Phase transfer entropy: A novel phase-based measure for directed connectivity in networks coupled by oscillatory interactions. *Neuroimage*. 2014;85:853-872. doi:10.1016/j.neuroimage.2013.08.056

35. Kudo K, Morise H, Ranasinghe KG, et al. Magnetoencephalography Imaging Reveals Abnormal Information Flow in Temporal Lobe Epilepsy. *https://home.liebertpub.com/brain*. August 2021. doi:10.1089/BRAIN.2020.0989

36. Oostenveld R, Fries P, Maris E, Schoffelen JM. FieldTrip: Open source software for advanced analysis of MEG, EEG, and invasive electrophysiological data. *Comput Intell Neurosci*. 2011;2011. doi:10.1155/2011/156869

37. Raj A, Cai C, Xie X, et al. Spectral graph theory of brain oscillations. *Hum Brain Mapp*. 2020;41(11):2980-2998. doi:10.1002/hbm.24991

38. Verma P, Nagarajan S, Raj A. Spectral graph theory of brain oscillations--Revisited and improved. *Neuroimage*. 2022;249. doi:10.1016/J.NEUROIMAGE.2022.118919

39. Moran R, Pinotsis DA, Friston K. Neural masses and fields in dynamic causal modelling. *Front Comput Neurosci*. 2013;0(APR 2013):57. doi:10.3389/FNCOM.2013.00057/BIBTEX

40. David O, Friston KJ. A neural mass model for MEG/EEG: coupling and neuronal dynamics. *Neuroimage*. 2003;20(3):1743-1755. doi:10.1016/J.NEUROIMAGE.2003.07.015

41. Ranasinghe KG, Verma P, Cai C, et al. Altered excitatory and inhibitory neuronal subpopulation parameters are distinctly associated with tau and amyloid in Alzheimer's disease. *bioRxiv*. March 2022:2022.03.09.483594. doi:10.1101/2022.03.09.483594

42. Wales DJ, Doye JPK. Global Optimization by Basin-Hopping and the Lowest Energy Structures of Lennard-Jones Clusters Containing up to 110 Atoms. *J Phys Chem A*. 1997;101(28):5111-5116. doi:10.1021/JP970984N

43. Thomas Yeo BT, Krienen FM, Sepulcre J, et al. The organization of the human cerebral cortex estimated by intrinsic functional connectivity. *J Neurophysiol*. 2011;106(3):1125-1165. doi:10.1152/jn.00338.2011

44. Brancaccio A, Tabarelli D, Bigica M, Baldauf D. Cortical source localization of sleep-stage specific oscillatory activity. *Sci Rep*. 2020;10(1):1-15. doi:10.1038/s41598-020-63933-5

45. Raichle ME, MacLeod AM, Snyder AZ, Powers WJ, Gusnard DA, Shulman GL. A default mode of brain function. *Proc Natl Acad Sci U S A*. 2001;98(2):676-682. doi:10.1073/pnas.98.2.676

46. Herbet G, Lafargue G, de Champfleur NM, et al. Disrupting posterior cingulate connectivity disconnects consciousness from the external environment. *Neuropsychologia*. 2014;56(1):239-244. doi:10.1016/j.neuropsychologia.2014.01.020

47. BA V, S L. Posterior cingulate, precuneal and retrosplenial cortices: cytology and components of the neural network correlates of consciousness. *Prog Brain Res*. 2005;150:205-217. doi:10.1016/S0079-6123(05)50015-3

48. Sämann PG, Wehrle R, Hoehn D, et al. Development of the brain's default mode network from wakefulness to slow wave sleep. *Cereb Cortex*. 2011;21(9):2082-2093. doi:10.1093/cercor/bhq295

49. Fernandez Guerrero A, Achermann P. Intracortical Causal Information Flow of Oscillatory Activity (Effective Connectivity) at the Sleep Onset Transition. *Front Neurosci*. 2018;12:912. doi:10.3389/fnins.2018.00912

50. Chow HM, Horovitz SG, Carr WS, et al. Rhythmic alternating patterns of brain activity distinguish rapid eye movement sleep from other states of consciousness. *Proc Natl Acad Sci U S A*. 2013;110(25):10300. doi:10.1073/PNAS.1217691110

51. Siclari F, Bernardi G, Riedner BA, LaRocque JJ, Benca RM, Tononi G. Two Distinct Synchronization Processes in the Transition to Sleep: A High-Density Electroencephalographic Study. *Sleep*. 2014;37(10):1621-1637. doi:10.5665/sleep.4070

52. Fernandez Guerrero A, Achermann P. Brain dynamics during the sleep onset transition: An EEG source localization study. *Neurobiol Sleep Circadian Rhythm*. 2019;6:24-34. doi:10.1016/j.nbscr.2018.11.001

53. Marzano C, Moroni F, Gorgoni M, Nobili L, Ferrara M, De Gennaro L. How we fall asleep: Regional and temporal differences in electroencephalographic synchronization at sleep onset. *Sleep Med*. 2013;14(11):1112-1122. doi:10.1016/j.sleep.2013.05.021

54. Werth E, Achermann P, Borbély AA. Fronto-occipital EEG power gradients in human sleep. *J Sleep Res*. 1997;6(2):102-112. doi:10.1046/j.1365-2869.1997.d01-36.x

55. Braun AR, Balkin TJ, Wesensten NJ, et al. Regional cerebral blood flow throughout the sleep-

wake cycle. An H215O PET study. *Brain*. 1997;120(7):1173-1197. doi:10.1093/brain/120.7.1173

56. Maquet. Functional neuroimaging of normal human sleep by positron emission tomography. *J Sleep Res*. 2000;9(3):207-231. doi:10.1046/j.1365-2869.2000.00214.x

57. Marzano C, Ferrara M, Curcio G, De Gennaro L. The effects of sleep deprivation in humans: Topographical electroencephalogram changes in non-rapid eye movement (NREM) sleep versus REM sleep. *J Sleep Res*. 2010;19(2):260-268. doi:10.1111/j.1365-2869.2009.00776.x

58. Hillebrand A, Barnes GR, Bosboom JL, Berendse HW, Stam CJ. Frequency-dependent functional connectivity within resting-state networks: An atlas-based MEG beamformer solution. *Neuroimage*. 2012;59(4):3909-3921. doi:10.1016/J.NEUROIMAGE.2011.11.005

59. Tagliazucchi E, von Wegner F, Morzelewski A, Brodbeck V, Laufs H. Dynamic BOLD functional connectivity in humans and its electrophysiological correlates. *Front Hum Neurosci*. 2012;6(DEC):339. doi:10.3389/fnhum.2012.00339

60. Boly M, Perlbarg V, Marrelec G, et al. Hierarchical clustering of brain activity during human nonrapid eye movement sleep. *Proc Natl Acad Sci U S A*. 2012;109(15):5856-5861. doi:10.1073/pnas.1111133109

61. Adamantidis AR, Herrera CG, Gent TC. Oscillating circuitries in the sleeping brain. *Nat Rev Neurosci 2019 2012*. 2019;20(12):746-762. doi:10.1038/s41583-019-0223-4

62. Nguyen T, Babawale O, Kim T, Jo HJ, Liu H, Kim JG. Exploring brain functional connectivity in rest and sleep states: a fNIRS study. *Sci Reports 2018 81*. 2018;8(1):1-10. doi:10.1038/s41598-018-33439-2

63. Rosenberg RS, Steven FAASM;, Hout V. The American Academy of Sleep Medicine Inter-scorer Reliability Program: Sleep Stage Scoring. *J Clin Sleep Med*. 2013;9(1):81-87. doi:10.5664/JCSM.2350

64. Stevner ABA, Vidaurre D, Cabral J, et al. Discovery of key whole-brain transitions and dynamics during human wakefulness and non-REM sleep. *Nat Commun*. 2019;10(1). doi:10.1038/s41467-019-08934-3

65. Altmann A, Schröter MS, Spoormaker VI, et al. Validation of non-REM sleep stage decoding from resting state fMRI using linear support vector machines. *Neuroimage*. 2016;125:544-555.

doi:10.1016/J.NEUROIMAGE.2015.09.072

66. Ogilvie RD. The process of falling asleep. *Sleep Med Rev*. 2001;5(3):247-270. doi:10.1053/SMRV.2001.0145

67. Goupil L, Bekinschtein TA. Cognitive processing during the transition to sleep. *Arch Ital Biol*. 2012;150(2/3):140-154. doi:10.4449/AIB.V150I2.1247

68. Hillebrand A, Tewarie P, Dellen E van, et al. Direction of information flow in large-scale resting-state networks is frequency-dependent. *Proc Natl Acad Sci*. 2016;113(14):3867-3872. doi:10.1073/PNAS.1515657113

69. Buzsáki G, Watson BO. Brain rhythms and neural syntax: implications for efficient coding of cognitive content and neuropsychiatric disease. *Dialogues Clin Neurosci*. 2012;14(4):345. doi:10.31887/DCNS.2012.14.4/GBUZSAKI

70. De Gennaro L, Vecchio F, Ferrara M, Curcio G, Rossini PM, Babiloni C. Changes in fronto-posterior functional coupling at sleep onset in humans. *J Sleep Res*. 2004;13(3):209-217. doi:10.1111/j.1365-2869.2004.00406.x

71. Vecchio F, Miraglia F, Gorgoni M, et al. Cortical connectivity modulation during sleep onset: A study via graph theory on EEG data. *Hum Brain Mapp*. 2017;38(11):5456-5464. doi:10.1002/hbm.23736

72. Bertini M, Ferrara M, De Gennaro L, et al. Directional information flows between brain hemispheres during presleep wake and early sleep stages. *Cereb Cortex*. 2007;17(8):1970-1978. doi:10.1093/cercor/bhl106

73. Fox MD, Raichle ME. Spontaneous fluctuations in brain activity observed with functional magnetic resonance imaging. *Nat Rev Neurosci*. 2007;8(9):700-711. doi:10.1038/nrn2201

74. Nikouline V V., Linkenkaer-Hansen K, Huttunen J, Ilmoniemi RJ. Interhemispheric phase synchrony and amplitude correlation of spontaneous beta oscillations in human subjects: A magnetoencephalographic study. *Neuroreport*. 2001;12(11):2487-2491. doi:10.1097/00001756-200108080-00040

75. Nir Y, Mukamel R, Dinstein I, et al. Interhemispheric correlations of slow spontaneous neuronal fluctuations revealed in human sensory cortex NIH Public Access Author Manuscript. *Nat*

*Neurosci*. 2008;11(9):1100-1108. doi:10.1038/nn.2177

76. Mantini D, Perrucci MG, Del Gratta C, Romani GL, Corbetta M. Electrophysiological signatures of resting state networks in the human brain. *Proc Natl Acad Sci U S A*. 2007;104(32):13170-13175. doi:10.1073/pnas.0700668104

77. Gamma A, Lehmann D, Frei E, Iwata K, Pascual-Marqui RD, Vollenweider FX. Comparison of simultaneously recorded [H215O]-PET and LORETA during cognitive and pharmacological activation. *Hum Brain Mapp*. 2004;22(2):83. doi:10.1002/HBM.20015

78. Vogt BA, Laureys S. Posterior Cingulate, Precuneal & Retrosplenial Cortices: Cytology & Components of the Neural Network Correlates of Consciousness. *Prog Brain Res*. 2005;150:205. doi:10.1016/S0079-6123(05)50015-3

79. Picchioni D, Duyn JH, Horovitz SG. Sleep and the functional connectome. *Neuroimage*. 2013;80:387-396. doi:10.1016/J.NEUROIMAGE.2013.05.067

80. Hassabis D, Kumaran D, Maguire EA. Using Imagination to Understand the Neural Basis of Episodic Memory. *J Neurosci*. 2007;27(52):14365-14374. doi:10.1523/JNEUROSCI.4549-07.2007

81. Herbet G, Lafargue G, Bonnetblanc F, Moritz-Gasser S, Menjot de Champfleur N, Duffau H. Inferring a dual-stream model of mentalizing from associative white matter fibres disconnection. *Brain*. 2014;137(3):944-959. doi:10.1093/BRAIN/AWT370

82. R H, H M, M R, et al. Human cortical excitability increases with time awake. *Cereb Cortex*. 2013;23(2):332-338. doi:10.1093/CERCOR/BHS014

83. Ly JQM, Gaggioni G, Chellappa SL, et al. Circadian regulation of human cortical excitability. *Nat Commun 2016 71*. 2016;7(1):1-10. doi:10.1038/ncomms11828

84. Miyawaki H, Diba K. Regulation of Hippocampal Firing by Network Oscillations during Sleep. *Curr Biol*. 2016;26(7):893-902. doi:10.1016/j.cub.2016.02.024

85. Vyazovskiy V V., Olcese U, Lazimy YM, et al. Cortical Firing and Sleep Homeostasis. *Neuron*. 2009;63(6):865-878. doi:10.1016/J.NEURON.2009.08.024

86. M M, F F, R H, SK E, H S, G T. Breakdown of cortical effective connectivity during sleep. *Science*. 2005;309(5744):2228-2232. doi:10.1126/SCIENCE.1117256

87. Massimini M, Ferrarelli F, Huber R, Esser SK, Singh H, Tononi G. Neuroscience: Breakdown of

cortical effective connectivity during sleep. *Science (80- )*. 2005;309(5744):2228-2232. doi:10.1126/science.1117256

88. R K, D N, T O, et al. Sensory perception during sleep in humans: a magnetoencephalograhic study. *Sleep Med*. 2003;4(6):493-507. doi:10.1016/S1389-9457(03)00169-2

89. RN S, FF E, CJ W. Effect of subthreshold up and down states on the whisker-evoked response in somatosensory cortex. *J Neurophysiol*. 2004;92(6):3511-3521. doi:10.1152/JN.00347.2004

90. M B, I T, M S, TJ S. Model of thalamocortical slow-wave sleep oscillations and transitions to activated States. *J Neurosci*. 2002;22(19):8691-8704. doi:10.1523/JNEUROSCI.22-19-08691.2002

91. Cardone P, Van Egroo M, Chylinski D, Narbutas J, Gaggioni G, Vandewalle G. Increased cortical excitability but stable effective connectivity index during attentional lapses. *Sleep*. 2021;44(6):1-11. doi:10.1093/SLEEP/ZSAA284

92. Civardi C, Boccagni C, Vicentini R, et al. Cortical excitability and sleep deprivation: a transcranial magnetic stimulation study. *J Neurol Neurosurg Psychiatry*. 2001;71(6):809-812. doi:10.1136/JNNP.71.6.809

93. Tamaki M, Wang Z, Barnes-Diana T, et al. Complementary contributions of non-REM and REM sleep to visual learning. *Nat Neurosci 2020 239*. 2020;23(9):1150-1156. doi:10.1038/s41593-020-0666-y

94. Bridi MCD, Zong FJ, Min X, et al. Daily Oscillation of the Excitation-Inhibition Balance in Visual Cortical Circuits. *Neuron*. 2020;105(4):621-629.e4. doi:10.1016/J.NEURON.2019.11.011

95. Diering GH, Nirujogi RS, Roth RH, Worley PF, Pandey A, Huganir RL. Homer1a drives homeostatic scaling-down of excitatory synapses during sleep. *Science (80- )*. 2017;355(6324):511-515. doi:10.1126/SCIENCE.AAI8355

96. Herman ST, Walczak TS, Bazil CW. Distribution of partial seizures during the sleep-wake cycle: Differences by seizure onset site. *Neurology*. 2001;56(11):1453-1459. doi:10.1212/WNL.56.11.1453

97. Bazil CW. Seizure modulation by sleep and sleep state. *Brain Res*. 2019;1703:13-17. doi:10.1016/j.brainres.2018.05.003

## FIGURE LEGENDS

**Figure 1. Spectral and spatial FC maps between sleep-wake states in the delta frequency band.** A) Mean relative spectral power, averaged across regions and patients in wake (purple), N1 (green), and N2 (orange). Light shading represents the standard error across patients. B) Spatial maps of relative spectral power in sleep-wake states. C) Spatial map of global synchrony in W, N1, and N2 within the delta band, as measured by imaginary coherence. D) T-score map of differences in regional FC between W and N1 within the delta band. Lobar regions delineated on x- and y- axis are further described in Table 1s. E) Top 50 highest positive functional connections, favoring N1. F) Mean relative spectral power of each sleep-wake state in the delta band, averaged across regions and patients. Error bars represent the 95% CI from the LS-mean. G) Mean long-range synchrony for each sleep-wake state in the delta band, averaged across region and patients. Error bars again denote 95% CI from the LS-mean. H) Association between averaged long-range synchrony (measured by mean imaginary coherence) and relative spectral power in the delta band. Each point represents an individual ROI within the spatial map. Linear regression and correlations of the averaged long-range synchrony and relative spectral power for individual ROIs are provided for within sleep-wake state and across state (black) populations.

**Figure 2. Spatial FC maps between sleep-wake states in the theta frequency band.** A) Spatial map of global synchrony in W, N1, and N2 within the theta band, as measured by imaginary coherence. B) T-score map of differences in regional FC between W and N1 within the theta band. C) Top 50 highest positive and negative functional connections, favoring N1 (red) and W (blue), respectively. D) Mean relative spectral power of each sleep-wake state in the theta band, averaged across regions and patients. Error bars represent the 95% CI from the LS-mean. E) Mean long-range synchrony for each sleep-wake state in the theta band, averaged across region and patients. Error bars again denote 95% CI from the LS-mean. F) Association between the spatial maps of mean global FC and relative spectral power in the theta band.

**Figure 3. Seeded study evaluating the FC between anterior and posterior regions of the DMN**. A) Voxels (red) that are involved and the anterior (*top*) and posterior (*bottom*) DMN. The anterior-posterior coupling as indicated by the arrows evaluates the interactions between anterior DMN voxels and posterior DMN voxels. B) Intrinsic FC within the anterior (*left*) and posterior (*middle*) DMN, and anterior-posterior coupling of the DMN (*right)* within the delta band and C) alpha band. Significance testing performed on multiple comparison testing across all regions (FDR level 0.5).

**Figure 4. Seeded study evaluating the FC between the PCC-precuneus and residual cortical structures (intercommunity) and within the PCC-precuneus (intrinsic)**. A) Voxels (red) that are involved in the PCC-precuneus with arrows indicating intercommunity (*top*) and intrinsic connectivity (*bottom*). B) FC relative to frequency bands for intercommunity and C) intrinsic connectivity.

**Figure 5. Directed information flow of sleep-wake states in the delta frequency band.** A-C) Directed FC as measured by directional phase transfer entropy (dPTE) across W, N1, and N2. From W to N1 and N2, there is increasing magnitude of dPTE with an aggregative inflow into the bilateral frontal regions. D-F) Alternate visualization of directed FC colored by orange (outflow) and purple arrow (inflow). The visualization across W, N1, and N2 using a common threshold for depicting increased magnitudes and trajectories of the directed FC. G-I) T-scores plotted indicating magnitude changes between specified states (accounting for FDR level 0.5)

**Figure 6. Biophysical NMM model across sleep-wake states demonstrated reduced excitation-inhibition with transition to sleep.** A) Depiction of NMM, comprised of both excitatory and inhibitory inputs and modeled with time constants ($\tau$) and gain ($g$) parameters. B) Optimized parameters of $\tau_e/\ \tau_i$ and $g_{ee}/g_{ii}$ across sleep-wake states. C) Excitatory-inhibitory ratios ($X_e/X_i$) across sleep-wake states, revealing an increased excitation-to-inhibition with transition from wake to sleep. D) Spatial maps of $X_e/X_i$ across sleep-wake states, revealing cortical heterogeneity in excitability. E) T-scores reflecting differences between N1 vs. W (*left*) and N2 vs. W (*right*) across

different ROIs. Depicted T-scores are thresholded to account for multiple comparison testing (FDR level 0.05). F) Actual (*top*) and modeled (*bottom*) power spectral density curves across sleep-wake states.